Korean J. Chem. Eng., 39(9), 2414-2423 (2022)
DOI: 10.1007/s11814-022-1094-3

pISSN: 0256-1115
eISSN: 1975-7220

Microwave-assisted pyrolysis of phosphoric acid-activated Goldenberry peel powder biochar for enhancing the adsorption of trace beta-lactamase inhibitors

Tian Ai*, Chunmei Xu, Lei Zhang*, Ke Chen*, Yonggui Wu***, Shujuan Dai****,†, Xiaolu Xiong*, Shixin Jie*, Xiaoni Jin*, and Zhongxu Yu*****

*School of Chemical Engineering, University of Science and Technology Liaoning, Anshan 114051, Liaoning, China
**Technical Development (Engineering) Department, Shandong Hualu Hengsheng Chemical Co., Ltd, Dezhou 253019, Shandong, China
***Technical Development (Engineering) Department, Hualu Hengsheng (JingZhou) Chemical Co., Ltd, Jingzhou 434100, Hubei, China
****School of Mining Engineering, University of Science and Technology Liaoning, Anshan 114051, Liaoning, China
(*Received 3 December 2021 • Revised 29 January 2022 • Accepted 23 February 2022*)

Abstract−Novel efficient biochar of Goldenberry peels (GBP_{MW}-H_3PO_4) was prepared through a microwave-assisted phosphoric acid activation method. It was characterized and used for removing two beta-lactamase inhibitors, sulbactam (SAM, first listed in Japan in 1986) and avibactam (AVI, first listed in the U.S. in 2015), from aqueous solution. Characterization confirmed that GBP_{MW}-H_3PO_4 displayed a high surface area (720.046 m^2 g^{-1}), more abundant pore structure, smaller particle size, and higher thermal stability. The experimental results showed that the adsorption of the two antibiotics was a spontaneous, favorable, and endothermic process, highly dependent on solution pH. A contact time of 60 min assured equilibrium, and GBP_{MW}-H_3PO_4 followed pseudo-first-order kinetics (R^2=0.9950-0.9977). Furthermore, the adsorption capacities of GBP_{MW}-H_3PO_4 for SAM and AVI were 211.86 and 198.81 mg g^{-1}, respectively, and the performance was better than that of unmodified biochar. Microscopically, the main mechanism could be explained by π-π electron donor-acceptor interaction, hydrogen bonding interaction, π-hydrogen bonding, hydrophobic interaction, and electrostatic interaction. The study demonstrates that the microwave-assisted H_3PO_4 activation method could produce biochar, and GBP_{MW}-H_3PO_4 was confirmed to be a low-cost and high-efficiency adsorbent for removing beta-lactamase inhibitors from medical wastewater.

Keywords: Microwave-assisted, Biochar, Beta-lactamase Inhibitors, Adsorption, Goldenberry Peel

INTRODUCTION

As one of the most important medical discoveries in early last century, antibiotics are widely used in medicine, modern aquaculture, and livestock production to prevent and treat bacterial infectious diseases [1,2]. Antibiotic residues are now regarded as emerging pharmaceutical contaminants in the water system [3]. In the past few decades, an increasing body of evidence has shown that antibiotics entering the various water environmental contexts, such as sewage or municipal wastewater, surface water, groundwater, and even drinking water, can threaten the ecological environment and even result in drug resistance of humans and animals [1,4]. Therefore, the World Health Organization (WHO) has categorized their spread as a serious public health problem, which has received extensive concern [5].

Beta-lactamase inhibitors, as a new class of beta-lactam antibiotic whose molecular structure contains a beta-lactam ring, are widely used to prevent and treat bacterial infections. Sulbactam sodium (SAM), invented by Barth at Pfizer in 1978, is a competitive, irreversible beta-lactamase inhibitor that acts as a synergist against Gram-positive bacteria and is effective for treating meningococcal and gonococcal diseases [6]. Avibactam sodium (AVI) is a novel synthetic beta-lactamase inhibitor without containing a beta-lactam core and has just come on the market for treating bacterial infections comprising Gram-negative organisms [7,8]. However, the presence of SAM and AVI in aquatic environments, even in low concentrations, can lead to the development of antibiotic-resistant bacteria, which significantly increases the potential risk to human health [9]. As a result, removing SAM and AVI from aquatic environments is particularly important at the societal level.

There are many methods for removing antibiotics from sewage water, such as physical treatment (e.g., filtration and flocculation), chemical treatment (e.g., photochemical degradation and ozonation), physic-chemical treatment (e.g., membrane separation and adsorption), and biological treatment (e.g., biodegradation and activated sludge) [10]. Adsorption, which is the transfer of a compound from the liquid phase to the solid phase, as been recognized as one of the most highly efficient techniques for removing low concentration antibiotics in practical applications, because of low expense, high efficiency, and easy operation [11].

In the research practice, the key to adsorption technology is to develop novel adsorbents. So far, biochar as an excellent adsorbent

†To whom correspondence should be addressed.
E-mail: Sunandshinesweet@163.com
Copyright by The Korean Institute of Chemical Engineers.

has come into notice due to its high cation exchange capacity, large porous structure, and abundant functional groups [12]. It is a thermal degradation product of various biomass, such as pine sawdust [13], rice straw [14], bamboo [15], and other crops, under an oxygen-limited atmosphere. Previous studies have shown that biochar is an effective adsorbent for antibiotics such as amoxicillin [16], tetracycline [16,17], chloramphenicol [17], cephalexin [18], sulfonamide [19], and oxytetracycline [20]. Note that some references have reported that biochar can adsorb beta-lactamase antibiotics in an aqueous solution, e.g., biochar from cornstalk can remove amoxicillin from aqueous solutions [21]. However, there are still few investigations in this area. It can be expected that biochar can significantly affect or even dominate the sorption of beta-lactamase inhibitors such as SAM and AVI [19].

At present, our research group has focused on the preparation of biochar from agricultural wastes with microwave-assisted chemical modification technology. It offers many unique superiorities, including quick start/stop, homogeneous non-contact heating, higher reaction rates, and better selectivity [22,23]. So far, various agricultural wastes such as sugarcane bagasse [24], pine sawdust [25], rice husk [26], and rapeseed shell [27] have been used as raw materials for preparing biochar using this technology.

Goldenberry, the common name of *Physalisalkengi L. var. franchetii* (Mast.) Makino, is an annual plant belonging to the Solanaceae family that is native to Heilongjiang, Jilin, Liaoning, and northeast Inner Mongolia in China. The peel of plant berries, considered a residue without a right destination, can cause blockages in waterways, especially during the rainy season. This high volume waste consists of appropriate lignocellulose. Thus, it can be potentially used as the source material of biochar.

New biochar from Goldenberry peels (GBP) was prepared by microwave-assisted chemical modification method for the first time in this work. It was characterized and tested for adsorption properties of beta-lactamase inhibitors, SAM and AVI (a class of emerging organic contaminants), from aqueous solutions. The specific objectives were to determine the effect of pH, contact time, initial antibiotic concentration, and temperature to understand SAM and AVI adsorption and mechanisms onto biochar. The corresponding adsorption kinetics, isotherms, and thermodynamics were also systematically evaluated. To the best of our knowledge, this is an innovative work, and its research findings will contribute to an improved understanding of the adsorption behavior of beta-lactamase inhibitors on biochar.

EXRERIMENTAL

1. Chemicals

For two Beta-lactamase inhibitors, SAM (>99.0% purity, CAS 69388-84-7) was purchased from Zhejiang Shengtong Biotechnology Co., Ltd. (Jinhua, China), and AVI (>98.0% purity, CAS 1192491-61-4) was obtained from Enantiotech Corporation Ltd. (Zhongshan, China). Both compounds were used as received without any further purification. Their chemical structures and detailed physicochemical parameters are summarized in Table S1 (Supplementary Information). All other chemicals, including adjusted pH of sample solutions and analysis of SAM and AVI, were supplied by Sinopharm Chemical Reagent Co., Ltd. (Shanghai, China), with analytical or HPLC grade agents used. All work solutions were prepared in ultra-pure water (18.2 MΩ cm^{-1}, 25 °C). Stock solutions of SAM (1,000 mg L^{-1}) and AVI (500 mg L^{-1}) were prepared in 1% methanol and kept in amber-colored bottles below 4 °C. The desired SAM and AVI concentrations used in the adsorption experiment were obtained by successive dilution of the pre-made stock solutions.

2. Preparation of Biochar by Microwave-assisted Treatment

GBP was obtained from a farmer's market in Anshan, Liaoning, China. The fruits were isolated by hand, and the peels were repeatedly rinsed with ultra-pure water to remove impurities. Then, they were dried in the shade for 10 days and milled until obtaining a particle size of 60 mesh, and finally stored in a tightly closed bottle for further use.

Biochar was prepared using a full-automatic microwave (model MDS-6G, Shanghai Sineo Microwave Chemistry Technology Co., Ltd., China). The process details were as follows: 0.5-g raw material was put in a 100-mL Teflon PFA (Perfluoroalkoxy) vessel, and 10-mL H_3PO_4 solution or ultra-pure water was added. The reaction tank containing the sample was placed into the microwave reactor by setting the temperature gradients of 150, 180, and 210 °C, and the reaction time of 30 min in total. At the end of this process, the reactor was withdrawn and then cooled to room temperature. The mixture was filtered and the desired solid product was purified with ultra-pure water until the pH value reached neutral. Finally, modified and unmodified biochar was dried in vacuum at 50 °C for 6 h, denoted as GBP_{MW}-H_3PO_4 and GBP_{MW}-H_2O, respectively. After weighing, the yields of the two biochars were about 51.23 and 42.50 wt%, respectively.

3. Characterization of Biochar

The biochar particle size and size distribution were measured by a laser particle analyzer (Malvern model Mastersizer 3000, England). The point of zero charge (pH_{PZC}) of two biochars was measured by a mass titration method using a digital pH meter (Rex Electric Chemical model PHS-3C, China). Ash content was determined by heating biochar in a muffle furnace (model GWL-XB, Luoyang Juxing Kiln Co., Ltd., China) at 750 °C for 6 h. C, H, and N contents were performed using an elemental analyzer (Elementar Vario MICRO cube, Germany), and O content was calculated based on a mass balance. P content in biochar was analyzed using an inductively coupled plasma optical emission spectrometer (Jena model PQ9000, Germany). The thermal stability of GBP_{MW}-H_3PO_4 and GBP_{MW}-H_2O was examined using a thermogravimetric analyzer (Netzsch model STA 449 F5 Jupiter, Germany) under N_2 gas at 25-1,000 °C at a heating rate of 10 °C min^{-1}. Textural characterization including the BET surface areas and pore structure analysis results of biochar samples was evaluated using N_2 gas adsorption/desorption isotherms at 77 K on a surface area analyzer (Quantachrome Autosorb iQ2, USA). The surface morphologies and elemental composition of prepared adsorbents were investigated by scanning electron microscopy (Zeiss model Sigma 500, Germany) equipped with energy dispersive spectroscopy (Bruker model XFlash 6-100, Germany). Finally, the potential changes in surface functional groups of adsorbents before and after adsorption were recorded and studied by a Fourier transform infrared (FTIR) spectrometer (Thermo model Nicolet 380, USA) to explain the possible adsorp-

tion mechanism.

4. Batch Adsorption Studies

In a typical adsorption experiment, a 25-mg biochar adsorbent was mixed with 50-mL beta-lactamase inhibitor aqueous solutions on a 150-mL stopper conical flask covered with tin foil paper. The flasks were shaken on a thermostatic orbital shaker (model SHZ-82B, Shanghai Jingaltar Instrument Manufacturing Co., Ltd., China) at 100 pm, and kept constant throughout the work. The suspension pH values were adjusted by dilute HCl or dilute NaOH solution. After adsorption equilibrium, the suspensions were immediately filtered through a 0.45-μm filter membrane, the remaining concentrations of SAM and AVI were monitored using a UV-vis spectrophotometer (Macy China Instruments Inc model UV-1300, China) at their maximum absorbance wavelength of 230 and 210 nm, respectively. Each experiment was performed in triplicate with relative standard deviations less than 5.0%. The equilibrium adsorption capacity of SAM and AVI, q_e (mg g^{-1}), could be determined using the following formula:

$$q_e = \frac{(C_0 - C_e)V}{W} \quad (1)$$

where C_0 and C_e are the initial and equilibrium antibiotics concentrations (mg L^{-1}), respectively; V is the solution volume (L); W the weight of prepared biochar (mg).

5. Adsorption Kinetics, Isotherms, and Thermodynamics

Many studies have used methods with much higher concentrations (mg L^{-1}) than that of actual environmental samples (μg L^{-1} or ng L^{-1}) to prove the effectiveness of biochar [19,28,29]. Batch experiments were performed to compare the adsorption of SAM and AVI onto the obtained biochars. First, the effect of varying pH on the adsorption of SAM and AVI onto biochar was investigated at pH 1.0-13.0, using an initial antibiotic concentration of 25 mg L^{-1} and a contact time of 180 min at 25 °C. The determined optimum pH was used in all the following experiments. For the kinetic study, the pre-determined time was controlled to be 0 to 300 min; initial antibiotics concentrations were maintained at 25 mg L^{-1}; the temperature was kept constant at 25 °C. In isotherm experiments, the initial antibiotics concentrations were in the range of 0.5 to 100 mg L^{-1} for each biochar. Other operating conditions were the same as above (with a contact time of 180 min at 25 °C). Furthermore, the thermodynamics experiments were performed at controlled temperatures of 20, 25, 30, 35, and 40 °C (with a contact time of 180 min and an initial antibiotics concentration of 25 mg L^{-1}).

Table 1. The kinetic, isotherm models, and thermodynamics equations used in this study

Models	Expression
Pseudo-first-order	$\ln(q_e - q_t) = \ln q_e - k_1 t$
Pseudo-second-order	$\frac{t}{q_t} = \frac{1}{k_2 q_e^2} + \frac{t}{q_e}$
Film diffusion	$\ln\left(1 - \frac{q_t}{q_e}\right) = -k_F t + A$
Intra-particle diffusion	$q_t = k_S t^{1/2} + C$
Langmuir	$\frac{C_e}{q_e} = \frac{1}{q_L K_L} + \frac{C_e}{q_L}$
Freundlich	$\ln q_e = \ln K_F + \frac{1}{n}\ln C_e$
Temkin	$q_e = \frac{RT}{\beta_T}\ln(K_T C_e)$
Dubinin-Radushkevich	$\ln q_e = \ln q_D - \left(\frac{RT}{\sqrt{2}E}\right)^2 \cdot \left(\ln\left(1 + \frac{1}{C_e}\right)\right)^2$
Van't Hoff	$K_C = q_e / C_e$ $\Delta G^o = -RT\ln K_C$ $\Delta G^o = \Delta H^o - T\Delta S^o$ $\ln K_C = \frac{\Delta S^o}{R} - \frac{\Delta H^o}{RT}$

6. Data Analysis

The experimental equilibrium data were analyzed to investigate the mechanisms of the SAM and AVI adsorption process using four adsorption kinetic models (pseudo-first-order, pseudo-second-order, intra-particle diffusion, and liquid film diffusion kinetic models), four most common adsorption isotherm models, (Langmuir, Freundlich, Temkin, and Dubinin-Radushkevich (D-R) isotherm models), and the three thermodynamic parameters (the standard Gibb's free energy (ΔG^o), the enthalpy change (ΔH^o), and the entropy change (ΔS^o)). The expressions for the employed models and equations are summarized in Table 1.

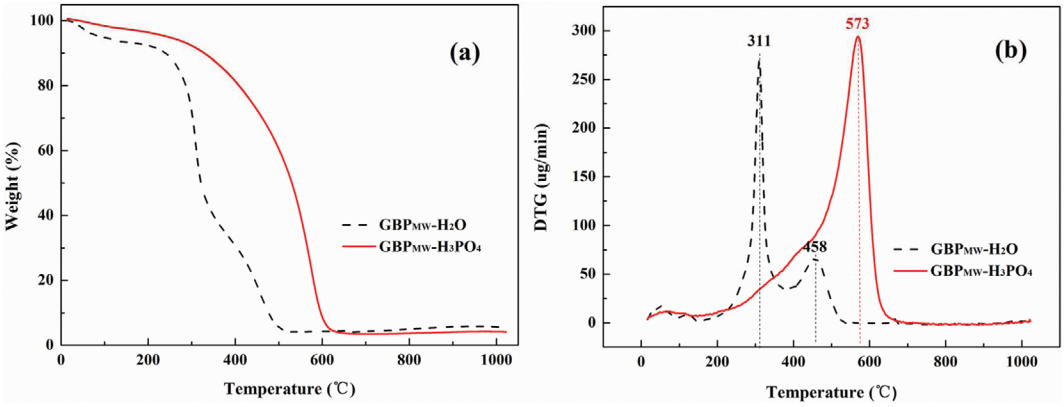

Fig. 1. (a) TG and (b) DTG profiles of GBP_{MW}-H_2O and GBP_{MW}-H_3PO_4.

RESULTS AND DISCUSSION

1. Characterization of Biochar Adsorbents

The pyrolytic characteristics of biochar before and after modification were monitored by thermal gravimetric-derivative thermogravimetric (TG-DTG) analysis at 1,000 °C (see Fig. 1 for the results). Fig. 1(a) shows that the final retention rates of 5.22 and 4.06% for GBP_{MW}-H_2O and GBP_{MW}-H_3PO_4 imply the continuous decomposition of hemicellulose and cellulose in biomass samples, respectively [22]. In the DTG curve of GBP_{MW}-H_2O, the first decomposition peak at 311 °C could be associated with the removal of hydroxyl groups of biomass (cellulose, hemicellulose, and lignin). The second broad peak at 458 °C was chiefly attributed to the decomposition of more heat-resistant components such as carboxyl or carbonyl groups during carbonization. After modification, only a new decomposition process (at 573 °C) emerged in the DTG curve of GBP_{MW}-H_3PO_4 due to the cross-linking reaction between phosphoric acid and biomass. Thus, the stability of biochar was improved.

Table S2 and Fig. S1 show the particle size distribution of GBP_{MW}-H_2O and GBP_{MW}-H_3PO_4. The mean particle sizes (D [3,2] and D [4,3]) of GBP_{MW}-H_3PO_4 are 35.4 and 72.4 μm with 16.2, 62.3, and 140 μm for Dx (10), Dx (50), and Dx (90), respectively, which are much smaller than those of GBP_{MW}-H_2O (72.4, 244, 40.8, 202, and 495 μm for D [3,2], D [4,3], Dx (10), Dx (50), and Dx (90), respectively). This indicates that the modification of phosphoric acid can significantly reduce the particle size of biochar.

Table 2 shows some of the physical and chemical properties of two types of biochars, including pH_{pzc} (with pH at the point of zero charge), elemental composition (%P, %C, %H, %O, and %N), and porous structure (BET surface area and pore volume). In Table 2, the pH_{pzc} of GBP_{MW}-H_2O and GBP_{MW}-H_3PO_4 are 5.60 and 4.55, respectively, suggesting that the biochar surface is positively charged at solution pH below pH_{pzc} and negatively charged at pH above pH_{pzc}.

Elemental analysis indicated that GBP_{MW}-H_2O and GBP_{MW}-H_3PO_4 were dominated by C (55.07 and 63.27%, respectively), followed by O (31.32 and 25.76%) and contained very little N (less 3.0%). Meanwhile, the measured %P using acid digestion in GBP_{MW}-H_2O was negligible while GBP_{MW}-H_3PO_4 had 11.11% of %P. The above results showed that two types of biochar were carbon-rich materials,

Table 2. The information of elemental composition of GBP_{MW}-H_2O and GBP_{MW}-H_3PO_4

Adsorbent		GBP_{MW}-H_2O	GBP_{MW}-H_3PO_4
Elemental compositions (%, mass based)	%C	55.07	63.27
	%H	6.37	5.53
	%N	2.80	1.10
	%S	0.30	0.34
	%O	31.32	25.76
	%P	N.D	0.58
Atom ratio	H/C	0.12	0.087
	O/C	0.57	0.41
Ash (%)		4.14	4.00
BET surface area (m^2 g^{-1})		368.670	720.046
Total pore volume (cm^3 g^{-1})		0.254	0.380
Micropore volume (cm^3 g^{-1})		0.110	0.243
Mesopore volume (cm^3 g^{-1})		0.144	0.137
Average of pore width (nm)		2.759	2.108
pH_{pzc}		5.60	4.55

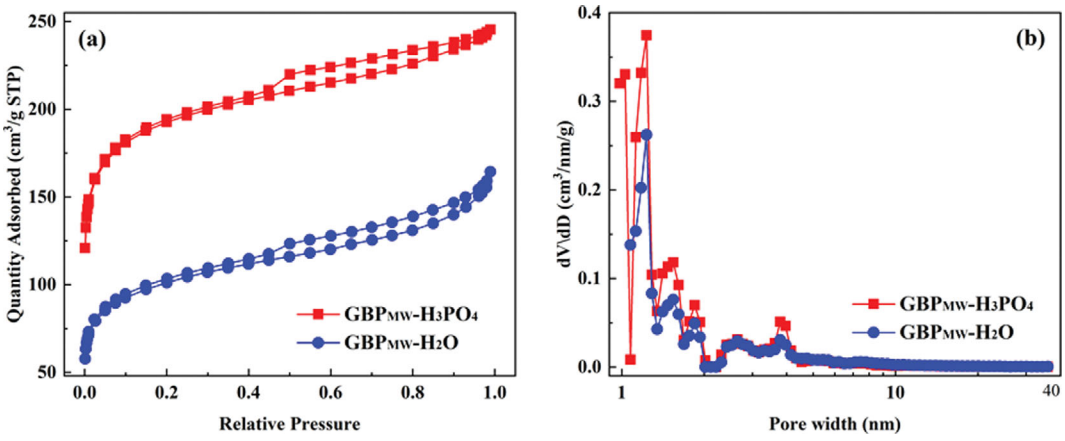

Fig. 2. (a) Nitrogen adsorption-desorption isotherms, (b) pore size distribution curves of GBP_{MW}-H_2O and GBP_{MW}-H_3PO_4.

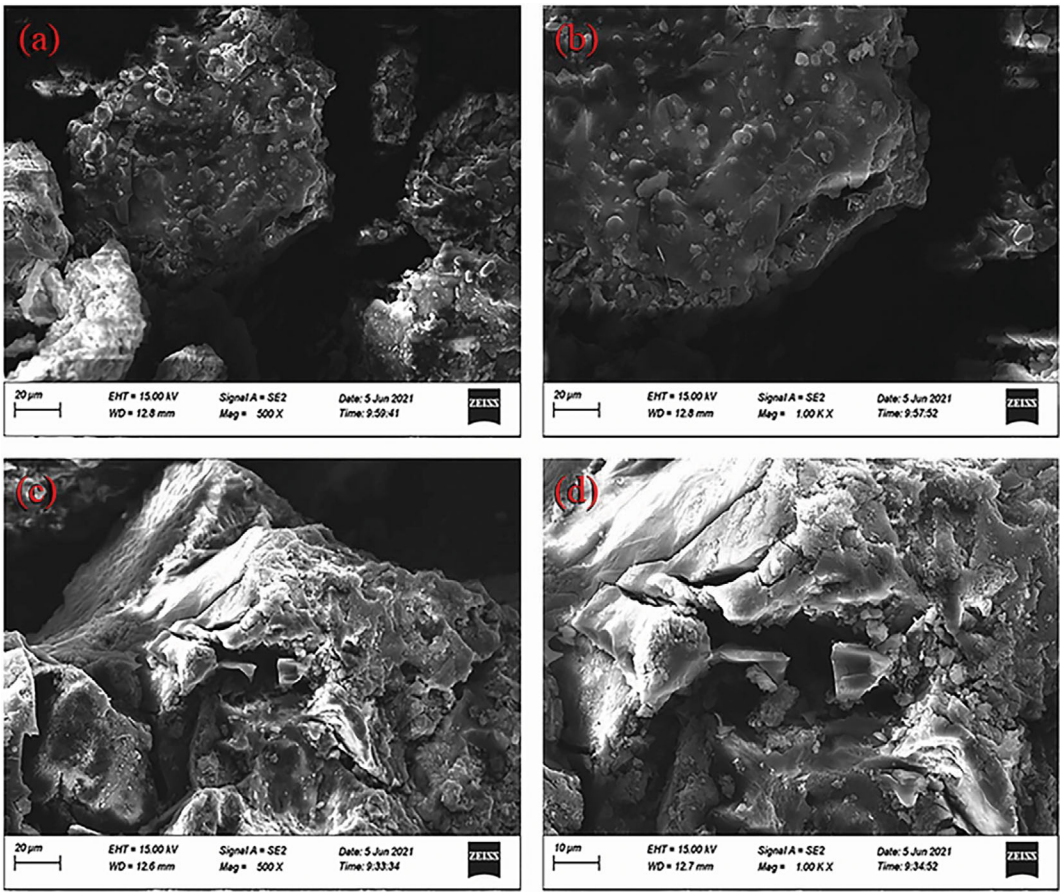

Fig. 3. SEM images of (a) and (b) GBP_{MW}-H_2O, (c) and (d) GBP_{MW}-H_3PO_4.

and P in GBP_{MW}-H_3PO_4 mainly came from the modifier, namely phosphoric acid. Besides, the r H/C and O/C values of 0.087 and 0.41 for GBP_{MW}-H_3PO_4 were relatively lower than those (0.12 and 0.57) of GBP_{MW}-H_2O, respectively, indicating that the biochar after microwave pyrolysis was highly carbonized and GBP_{MW}-H_3PO_4 had a higher hydrophobicity than GBP_{MW}-H_2O. After H_3PO_4 activation, the BET surface area, micropore volume, and mesopore volume of prepared biochar increased from 368.670 $m^2\ g^{-1}$, 0.110 $cm^3\ g^{-1}$, and 0.144 $cm^3\ g^{-1}$ to 720.046 $m^2\ g^{-1}$, 0.243 $cm^3\ g^{-1}$, and 0.137 $cm^3\ g^{-1}$, respectively. Thus, microwave radiation was favorable for the hydrolysis of GBP, and H_3PO_4 activation could make biochar have a large number of pores and channels and convert a small fraction of mesopores into micropores, which provides a basis for the superior adsorption performance of GBP_{MW}-H_3PO_4 [30].

Figs. 2(a) and (b) show the nitrogen adsorption-desorption isotherms and pore size distributions of two types of biochar, respectively. According to the International Union of Pure and Applied Chemistry (IUPAC) nomenclature, the measured isotherms exhibit a type I pattern with the type H4 hysteresis loop, which is a typical feature of biochar adsorbent for micropore and mesopore filling [31]. The preparation of biochar-rich microporous structures in the work is particularly beneficial to the adsorption of low- to medium-sized pharmaceutical molecules, which has also been discussed in several previous studies [13,32,33].

The surface morphology and elemental composition of GBP_{MW}-H_2O and GBP_{MW}-H_3PO_4 were examined by SEM equipped with an EDX system. Fig. 3 illustrates two successive magnifications (x500 and x1,000) of the tested samples. The two types of biochar are porous, and GBP_{MW}-H_2O shows an irregularly smooth surface and chunked book-like layer structure with groove-like valleys on its side. Compared with GBP_{MW}-H_2O, the surface texture of GBP_{MW}-H_3PO_4 becomes rougher, and the pores develop into the interior with an abundant ravine. The pores can be partly attributed to phosphoric acid etching during microwave activation and can serve as an active adsorption site to enable beta-lactamase inhibitors molecules into biochar. Moreover, the element composition proportion (O and P) of GBP_{MW}-H_3PO_4 is determined by EDS elemental mapping. Fig. S2 shows the content ratio of O to P is 10 : 1, indicating that P has significant residues in modified biochar as an activator.

2. Effect of pH on the Adsorption of SAM and AVI

Solution pH can significantly affect the adsorption process because it changes the ionization forms of adsorbates and the surface charge density of biochar [28,34]. Fig. 4 shows the effects of initial solution pH on the adsorption capacities of GBP_{MW}-H_2O and GBP_{MW}-H_3PO_4 for SAM and AVI. GBP_{MW}-H_3PO_4 and GBP_{MW}-H_2O present a similar trend, but the adsorption capacity of the former is much higher than that of the latter. Their adsorption increases with initial solution pH from 1 to 4, and the maximum adsorption capacities of SAM and AVI (48.57 and 49.48 mg g^{-1} for GBP_{MW}-

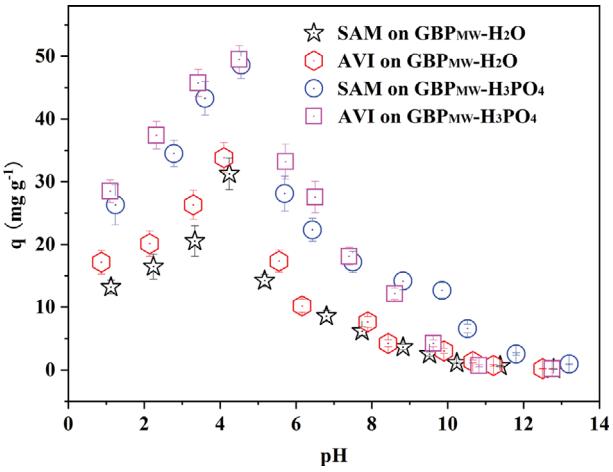

Fig. 4. Effect of equilibrium pH on adsorption of SAM and AVI by GBP_{MW}-H_2O and GBP_{MW}-H_3PO_4. Conditions: contact time 120 min, temperature 25 °C and initial drug concentrations 25 mg L^{-1}.

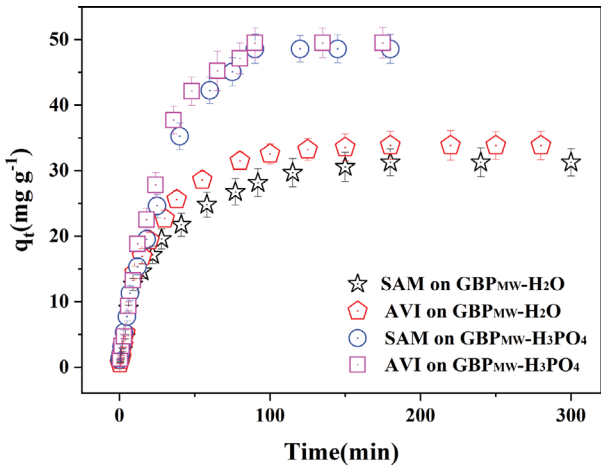

Fig. 5. Effect of contact time on adsorption of SAM and AVI by GBP_{MW}-H_2O and GBP_{MW}-H_3PO_4. Conditions: pH 4.0, temperature 25 °C and initial drug concentrations 25 mg L^{-1}.

H_3PO_4, and 31.25 and 33.82 mg g^{-1} for GBP_{MW}-H_2O) occur at about pH 4.0. However, it decreases slightly as pH further increases, and the adsorption capacity sharply declines when pH exceeds 8.0. Combined with the zero-point potential analysis, electrostatic interaction may be one of the adsorption mechanisms.

The pH_{PZC} of GBP_{MW}-H_3PO_4 and GBP_{MW}-H_2O was found around 4.0-5.0, suggesting that the surface of two biochars is electropositive when pH<4.0, and then converted to the electronegative state as the pH value increases. SAM and AVI are negative ions in aqueous solutions according to their structural properties. When the pH value of the solution is lower than 4.0 (pH_{PZC}), the electrostatic interaction between adsorbate and biochar is mainly electrostatic attraction, thus with remarkable adsorption. Interestingly, excellent adsorption near to pH_{PZC} indicates additional adsorption mechanisms, i.e., hydrogen bonding, electron donor-acceptor, and π-π dispersion interaction [34]. It can be summarized as follows: (1) The presence of oxygen-containing groups on the biochar facilitates the adsorption through hydrogen bonding [35]; (2) carboxyl groups on the biochar can be used as electron acceptors, while -OH and P-O groups are used as electron donors [36]. After pH passes the optimal value, the negative charge on the surface of two types of biochar gradually increases, so adsorption is less favorable due to increased electrostatic repulsion [28]. It can be hypothesized that abundant hydroxide ions (OH^-) have a competitive effect with pharmaceutical anions under alkaline conditions, resulting in a substantial decrease of adsorption capacity [11,37]. On the whole, the changes in pH have predominant effects on the adsorption of SAM and AVI, depending on the balance between attractive and repulsive forces. The adsorption mechanism will be discussed in detail in a separate chapter. Therefore, pH 4.0 is considered as the optimum and selected for the subsequent experiments.

3. Adsorption Kinetics

Fig. 5 shows the evolution of SAM and AVI adsorption versus time onto GBP_{MW}-H_2O and GBP_{MW}-H_3PO_4. All adsorption processes reach equilibrium in a really short time, and approximately 80-90% of equilibrium SAM and AVI uptake is adsorbed within the first 60 min. This excellent performance can be ascribed to the abundant availability of active sites and the high driving force in the mass transfer. Adsorption is presumed to occur on the external surface of biochar [13,38,39]. Afterward, adsorption gradually increases and finally reaches equilibrium within 180 and 90 min for GBP_{MW}-H_2O and GBP_{MW}-H_3PO_4, respectively.

Adsorption kinetic models can evaluate the relationship between the structure of biochar and adsorption performance in terms of the order of rate constants [10,40]. Table S3 and Fig. S3 present the linearized fitting forms of pseudo-first-order and pseudo-second-order kinetic models as well as the kinetic parameters and the correlation coefficients (R^2) of each model.

For GBP_{MW}-H_3PO_4, the fitting of the pseudo-second-order model fails because of the low R^2 (R^2=0.9285-0.9747) and large Δq(%) (Δq= 22.31-37.50%). Compared with the pseudo-second-order model, the pseudo-first-order model provides a more comprehensive reflection of the adsorption mechanism of SAM and AVI due to high R^2 (R^2=0.9950-0.9977) and low Δq(%) (Δq=1.43-1.77%). For GBP_{MW}-H_2O, the experimental data fit well with pseudo-first-order and pseudo-second-order kinetic models, indicating both physisorption and chemisorption mechanisms occur for this adsorption system [41]. The above results prove that physisorption is the rate-controlling step, and hydrophobic interaction and π-π dispersion interaction may act simultaneously in adsorbing SAM and AVI on biochar.

4. Adsorption Isotherm

Typical isotherm models, Langmuir, Freundlich, Temkin, and D-R models, were used to correlate the equilibrium isotherm data obtained from adsorbing SAM and AVI onto GBP_{MW}-H_2O and GBP_{MW}-H_3PO_4 for the initial concentrations of 0.5-100 mg L^{-1}. Table S4 summarizes the fitting parameters (q_L, K_L, K_F, n, K_T, β_D, q_D, and E) and correlation coefficients (R^2) calculated from four equations of the model.

Langmuir and Freundlich equations provided the optimal fitting results, followed by Temkin and D-R models. However, the fitting

Table 3. Comparison of the maximum adsorption capacities for beta-lactam antibiotics with various porous materials

Adsorbent	Abbreviation	Beta-lactam antibiotics	q_m (mg g^{-1})	References
Goldenberry peel powder	GBP_{MW}-H_2O	Sulbactam	42.50	This study
		Avibactam	49.83	
	GBP_{MW}-H_3PO_4	Sulbactam	211.86	
		Avibactam	198.81	
Ion exchange resin	A microparticles	Cefotaxime	962.07	[43]
	T1 microparticles		1,029.46	
	T2 microparticles		980.39	
Activated sludge	N/A	Penicillin G	330	[44]
R. arrhizus	N/A		459	
Activated carbon	N/A		375	
Giant reed-carbon	KAC	Amoxicillin	345.4	[3]
Commercial carbon	CAC		250.7	
Gain reed	N/A		75.8	
Montmorillonite organoclay	DDAB-MT	Penicillin G	23.0	[45]
		Nafcillin	25.4	
		Cefotamime	26.2	
		Cefotaxime	37.714	
CdS-MWCNT nanocomposites	N/A	Cefradine	40.525	[46]
		Cefazolin	34.512	
NH_4Cl-induced activated carbon	NAC	Amoxicillin	438.6	[47]
Standard activated carbon	SAC		261.8	

of the data using the Temkin (R^2=0.8063-0.9561) and D-R (R^2= 0.8297-0.9028) isotherm models was not ideal; thus, it was not considered. For GBP_{MW}-H_2O, the Langmuir model (R^2=0.9983 for SAM and 0.9967 for AVI) fit the data of adsorption isotherms better than the Freundlich model (R^2=0.9566 for SAM and 0.9490 for AVI), implying the homogeneous and monolayer nature of SAM and AVI adsorption on the biochar surface. However, for GBP_{MW}-H_3PO_4, the Freundlich model was more suitable for adsorption (R^2=0.9937 for SAM and 0.9917 for AVI) than the Langmuir model (R^2=0.9623 for SAM and 0.9555 for AVI), suggesting multiple adsorption processes and heterogeneous adsorption sites. Based on the Langmuir model, the maximum adsorption capacities of SAM and AVI on GBP_{MW}-H_3PO_4 were reported as 211.86 and 198.81 mg g^{-1}, respectively. Biochar prepared by microwave activation could improve its adsorption capacity for SAM and AVI by 4 and 5 times, respectively. Overall, the adsorption of GBP_{MW}-H_3PO_4 was more diversified than GBP_{MW}-H_2O by comparing the parameters between the two types of biochar [42]. Table 3 compares the maximum adsorption capacity of beta-lactam antibiotics with some other adsorbents reported in the literature. According to the authors, GBP_{MW}-H_3PO_4 can be considered an efficient and promising adsorbent for removing beta-lactamase inhibitors.

5. Adsorption Thermodynamics

The thermodynamic parameters (ΔG^o, ΔH^o, and ΔS^o) were used to explore the spontaneity and characteristics of the adsorption process. Table S5 summarizes the calculated values.

All ΔG^o values were negative at 293, 298, 303, 308, and 313 K, indicating that the adsorption of SAM and AVI by GBP_{MW}-H_3PO_4 and GBP_{MW}-H_2O was spontaneous and favorable at the studied temperature. Meanwhile, as the adsorption temperature increased, ΔG^o values became more negative, confirming that the adsorption of SAM and AVI was more likely to occur at higher temperature. Furthermore, the positive ΔH^o values revealed the typical endothermicity of adsorbing SAM and AVI onto GBP_{MW}-H_3PO_4 and GBP_{MW}-H_2O [48]. Positive ΔS^o values showed the increased randomness of beta-lactamase inhibitors' adsorbed state at the adsorbent-solution interface and the degree of freedom in the adsorption process [30].

6. Mechanism of Adsorption

The kinetic data were analyzed using the intra-particle diffusion model and liquid film diffusion model to determine the type of rate-controlling step. Table S6 and Table S7 list the plots obtained for models and all parameters (k_{id}, A, k_{S1}, k_{S2}, k_{S3}, C_1, C_2, and C_3).

In Fig. S4, all intra-particle diffusion plots exhibit multilinearity, and these three linear segments do not pass through the origin, suggesting that diffusion within the channel is involved in the adsorption process, and the diffusion steps are controlled by other adsorption processes, such as boundary layer diffusion, surface adsorption, and external mass transfer.

Subsequently, the liquid film diffusion kinetic model is used to predict the possible diffusion mechanism. In all cases, the plots present good linearity (R^2>0.99) and the intercept is almost zero (–0.150~ +0.025), indicating that the rate-limiting step is mainly the diffusion of antibiotic molecules on the biochar surface from the bulk liquid phase [10]. Similar results were obtained by Yan et al. [49] who used $ZnCl_2$ modified biochar derived from aerobic granular sludge to remove tetracycline.

Some literature has reported that the adsorption of antibiotic molecules onto the adsorbents is closely related to the active groups and chemical bonds on their surface [50-52]. The FTIR spectra of

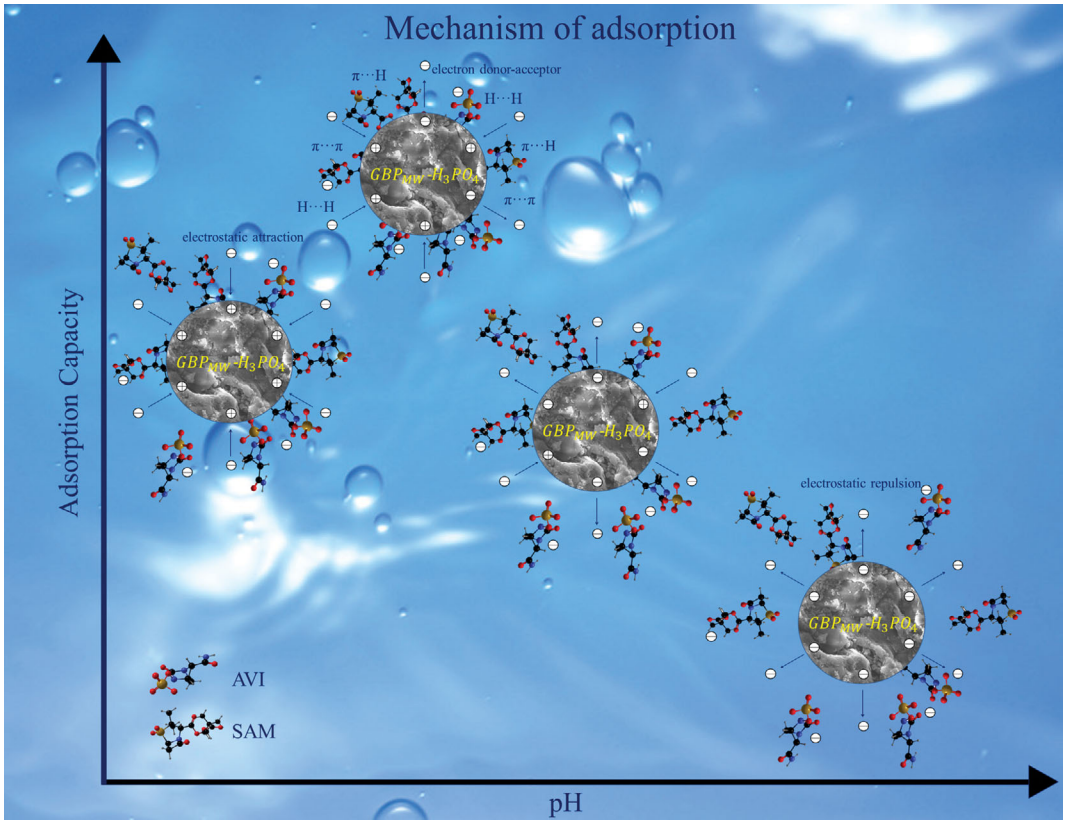

Fig. 6. The possible adsorption mechanism for SAM and AVI on GBP_{MW}-H_3PO_4.

GBP_{MW}-H_3PO_4 before and after adsorption of SAM and AVI were analyzed in the wavelength of 4,000-400 cm^{-1} to elucidate the adsorption mechanism of beta-lactamase inhibitors on the biochar (see Fig. S5 for results).

From the FTIR spectrum, the characteristic peaks of SAM were mainly located at 1,000-1,700 cm^{-1}. Namely, the peak at 1,654 and 1,401 cm^{-1} corresponded to the amino group and the sulfonyl group, respectively, and the peak near 1,152 cm^{-1} correlated to the ether bond. The spectrum of AVI was characterized by three bands at 1,600-1,700, 1,200-1,300, and 1,000-1,100 cm^{-1}. The peak at 1,754 and 1,678 cm^{-1} was ascribed to the C=O stretching of ester and amide. The peak at 1,243 cm^{-1} was ascribed to the C-O stretching, and the peak at 1,032 cm^{-1} corresponded to C-N stretching. After adsorbing SAM or AVI by GBP_{MW}-H_3PO_4, the main functional groups shifted at 3,143-3,461, 1,638-1,651 cm^{-1}, and 1,402-1,407 cm^{-1}, which represented O-H bond, C=C bond, and C-H bond stretching vibrations, respectively. Thus, the shifts of these peaks reflected the significant contribution on adsorption sites of these functional groups on the GBP_{MW}-H_3PO_4 surface [53]. From the above analysis and discussion, π-π electron donor-acceptor (EDA) interaction, hydrogen bonding interaction, and π-hydrogen bonding could be the main adsorption mechanism.

In addition to the above mechanisms, the adsorption of SAM and AVI on GBP_{MW}-H_3PO_4 was regulated by hydrophobic interaction and electrostatic interaction. Both interactions played an important role because SAM and AVI adsorption was a pH-dependent process (see Section 3.2). Simultaneously, the proposed adsorption mechanism was consistent with the results of the kinetic and thermodynamic analysis. Fig. 6 shows a possible reaction mechanism of GBP_{MW}-H_3PO_4 adsorbing SAM and AVI.

7. Desorption and Reuse of Biochar

From an economic perspective, the availability of reusable biochar is an important factor in reducing the costs of the process [54]. The adsorption/desorption (A/D) experiments were performed

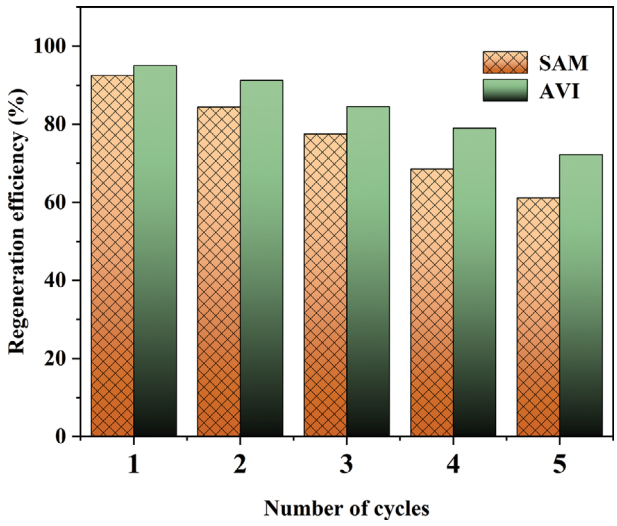

Fig. 7. Adsorption-desorption cycles of GBP_{MW}-H_2O and GBP_{MW}-H_3PO_4.

five times using the same biochar, and methanol was selected as a regeneration agent for each cycle experiment to explore the regeneration of GBP_{MW}-H_3PO_4. Fig. 7 shows the variation curve of the adsorption capacities of SAM and AVI adsorbed on GBP_{MW}-H_3PO_4 through five sequential A/D cycles. The regeneration efficiency decreases slowly during five cycles, indicating the material is an efficient adsorbent with excellent stability and reusability.

8. Cost of Adsorbents

GBP of the cheapest variety costs about CNY 320/ton. The modified material used in is the work was phosphoric acid at CNY 5,000/ton. The finished products cost approximately CNY 1,100/ton for GBP_{MW}-H_3PO_4 including all expenses (transportation, handling, electrical, energy, and drying). Compared with the traditional adsorption material activated carbon (at least CNY 3,000/ton), the cost of biochar prepared by microwave was much lower and the production process was more environmentally friendly.

CONCLUSIONS

GBP_{MW}-H_3PO_4 with high adsorption capacity for SAM and AVI was prepared by the microwave-assisted H_3PO_4 activation method for the first time. A large amount of phosphorus-containing functional groups was introduced on the biochar surface, which promoted the adsorption affinity toward SAM and AVI. Moreover, the BET surface area increased from 368.670 to 720.046 $m^2 g^{-1}$. Kinetics, isotherms, and thermodynamic studies exhibited that the adsorption process was spontaneous and endothermic, mainly affected by physisorption, and the rate of this process was controlled by multiple steps. Moreover, the adsorption mechanism, involving electrostatic interaction, π-π EDA interactions, hydrophobic force, and hydrogen bonds, depended on the changes in solution pH values. Most significantly, GBP_{MW}-H_3PO_4 could be regenerated and reused for removing SAM and AVI over five recycle steps. Based on all of these superior properties, the newly developed GBP_{MW}-H_3PO_4 as an effective adsorbent shows great potential application in removing emerging organic contaminants as beta-lactamase inhibitors from wastewater.

ACKNOWLEDGEMENTS

This work was financially supported by the National Natural Science Foundation of China (Grant Nos. 52174254, 51874168 and 51574146) and Xingliao Talents Science and Technology Innovation Leading Talents Project (Grant Nos. XLYC2002028).

DECLARATION OF COMPETING INTEREST

The authors declare that they have no known competing financial interests or personal relationships that could have appeared to influence the work reported in this paper.

SUPPORTING INFORMATION

Additional information as noted in the text. This information is available via the Internet at http://www.springer.com/chemistry/journal/11814.

REFERENCES

1. W. Yu, S. Zhan, Z. Shen, Q. Zhou and D. Yang, *Chem. Eng. J.*, **313**, 836 (2017).
2. Y. Wang, W. B. Jiao, J. T. Wang, G. F. Liu, H. L. Cao and J. Lü, *Bioresour. Technol.*, **277**, 128 (2019).
3. M. A. Chayid and M. J. Ahmed, *Chem. Eng.*, **3**, 1592 (2015).
4. B. Chen, W. Sun, C. Wang and X. Guo, *Chem. Eng. J.*, **316**, 160 (2017).
5. A. A Inyinbor, O. S. Bello, A. E. Fadiji and H. E. Inyinbor, *Chem. Eng.*, **6**, 784 (2017).
6. https://www.chemicalbook.com/ProductChemicalPropertiesCB1419201_EN.htm.
7. D. E. Ehmann, H. Jahic, P. L. Ross, R. F. Gu, J. Hu, G. Kern, G. K. Walkup and S. L. Fisher, *Proc. Natl. Acad. Sci. U.S.A.*, **109**, 11663 (2012).
8. Y. Wang, J. Wang, R. Wang, Y. Cai and J. Glob. *Antimicrob. Resist.*, **22**, 18 (2020).
9. S. Li, X. Zhang and Y. Huang, *J. Hazard. Mater.*, **321**, 711 (2017).
10. Q. Song, Y. Fang, Z. Liu, L. Li, Y. Wang, J. Liang, Y. Huang, J. Lin, L. Hu, J. Zhang and C. Tang, *Chem. Eng. J.*, **325**, 71 (2017).
11. S. Zhang, Y. Dong, Z. Yang, W. Yang, J. Wu and C. Dong, *Chem. Eng. J.*, **304**, 325 (2016).
12. Y. Shi, H. Hu and H. Ren, *Bioresour. Technol.*, **297**, 122281 (2020).
13. F. Reguyal, A. K. Sarmah and W. Gao, *J. Hazard. Mater.*, **321**, 868 (2017).
14. Y. Zhang, X. Yue, W. Xu, H. Zhang and F. Li, *J. Hazard. Mater.*, **379**, 120783 (2019).
15. R. Z. Wang, D. L. Huang, Y. G. Liu, C. Zhang, C. Lai, G. M. Zeng, M. Cheng, X. M. Gong, J. Wan and H. Luo, *Bioresour. Technol.*, **261**, 265 (2018).
16. A. Yazidi, M. Atrous, F. E. Soetaredjo, L. Sellaoui, S. Ismadji, A. Erto, A. Bonilla-Petriciolet and G. L. Dotto, *Chem. Eng. J.*, **379**, 122320 (2020).
17. P. Liao, Z. Zhan, J. Dai, X. Wu, W. Zhang, K. Wang and S. Yuan, *Chem. Eng. J.*, **228**, 496 (2013).
18. W. A. Khanday, M. J. Ahmed, P. U. Okoye, E. H. Hummadi and B. H. Hameed, *Bioresour. Technol.*, **280**, 255 (2019).
19. M. B. Ahmed, J. L. Zhou, H. H. Ngo, W. Guo, M. A. H. Johir and K. Sornalingam, *Chem. Eng. J.*, **311**, 348 (2017).
20. M. Jia, F. Wang, Y. Bian, X. Jin, Y. Song, F. O. Kengara, R. Xu and X. Jiang, *Bioresour. Technol.*, **136**, 87 (2013).
21. H. Li, J. Hu, Y. Cao, X. Li and X. Wang, *Bioresour. Technol.*, **246**, 168 (2017).
22. J. Qu, X. Tian, Z. Jiang, B. Cao, M. S. Akindolie, Q. Hu, C. Feng, Y. Feng, X. Meng and Y. Zhang, *J. Hazard. Mater.*, **387**, 121718 (2020).
23. Y. Li, N. Tsend, T. Li, H. Liu, R. Yang, X. Gai, H. Wang and S. Shan, *Bioresour. Technol.*, **273**, 136 (2019).
24. Y. H. Tang, S. H. Liu and D. C. W. Tsang, *J. Hazard. Mater.*, **383**, 121192 (2020).
25. C. R. Ellison, R. Hoff, C. Marculescu and D. Boldor, *Appl. Energy*, **259**, 114217 (2020).
26. N. Shukla, D. Sahoo and N. Remya, *J. Cleaner Prod.*, **235**, 1073 (2019).
27. G. Rao, S. Huang, U. Ashraf and Z. Mo, *Ecotoxicol. Environ. Saf.*, **185**, 109659 (2019).

28. P. Zhang, Y. Li, Y. Cao and L. Han, *Bioresour. Technol.*, **285**, 121348 (2019).
29. Z. Feng, K. Odelius, G. K. Rajarao and M. Hakkarainen, *Chem. Eng. J.*, **346**, 557 (2018).
30. J. Akhtar, N. S. Amin and A. Aris, *Chem. Eng. J.*, **170**, 136 (2011).
31. X. Zhu, C. Li, J. Li, B. Xie, J. Lü and Y. Li, *Bioresour. Technol.*, **263**, 475 (2018).
32. W. A. Khanday, M. J. Ahmed, P. U. Okoye, E. H. Hummadi and B. H. Hameed, *Bioresour. Technol.*, **280**, 255 (2019).
33. D. Mohan, A. Sarswat, V. K. Singh, M. Alexandre-Franco and C. U. Pittman, *Chem. Eng. J.*, **172**, 1111 (2011).
34. L. Lonappan, T. Rouissi, S. K. Brar, M. Verma and R. Y. Surampalli, *Bioresour. Technol.*, **249**, 386 (2018).
35. L. Zheng, Z. Dang, X. Yi and H. Zhang, *J. Hazard. Mater.*, **176**, 650 (2010).
36. W. Yang, Y. Lu, F. Zheng, X. Xue, N. Li and D. Liu, *Chem. Eng. J.*, **179**, 112 (2012).
37. K. W. Jung, S. Lee and Y. J. Lee, *Bioresour. Technol.*, **245**, 751 (2017).
38. L. Spessato, K. C. Bedin, A. L. Cazetta, I. P. A. F. Souza, V. A. Duarte, L. H. S. Crespo, M. C. Silva, R. M. Pontes and V. C. Almeida, *J. Hazard. Mater.*, **371**, 499 (2019).
39. H. Li, X. Dong, E. Silva, L. D. Oliveira, Y. Chen and L. Q. Ma, *Chemosphere*, **178**, 466 (2017).
40. A. C. Martins, O. Pezoti, A. L. Cazetta, K. C. Bedin, D. A. S. Yamazaki, G. F. G. Bandoch, T. Asefa, J. V. Visentainer and V. C. Almeida, *Chem. Eng. J.*, **260**, 291 (2015).
41. E. K. Putra, R. Pranowo, J. Sunarso, N. Indraswati and S. Ismadji, *Water Res.*, **43**, 2419 (2009).
42. Y. Zhao, W. Li, J. Liu, K. Huang, C. Wu, H. Shao, H. Chen and X. Liu, *Chem. Eng. J.*, **326**, 745 (2017).
43. S. Vasiliu, I. Bunia, S. Racovita and V. Neagu, *Carbohydr. Polym.*, **85**, 376 (2011).
44. Z. Aksu and Ö. Tunç, *Process Biochem.*, **40**, 831 (2005).
45. T. Saitoh and T. Shibayama, *J. Hazard. Mater.*, **317**, 677 (2016).
46. A. Fakhri, S. Rashidi, M. Asif, I. Tyagi, S. Agarwal and V. K. Gupta, *J. Mol. Liq.*, **215**, 269 (2016).
47. G. Moussavi, A. Alahabadi, K. Yaghmaeian and M. Eskandari, *Chem. Eng. J.*, **217**, 119 (2013).
48. M. F. Li, Y. G. Liu, S. B. Liu, D. Shu, G. M. Zeng, X. J. Hu, X. F. Tan, L. H. Jiang, Z. L. Yan and X. X. Cai, *Chem. Eng. J.*, **319**, 219 (2017).
49. L. Yan, Y. Liu, Y. Zhang, S. Liu, C. Wang, W. Chen, C. Liu, Z. Chen and Y. Zhang, *Bioresour. Technol.*, **297**, 122381 (2019).
50. H. Zhao, X. Liu, Z. Cao, X. Shi, Y. Yang, J. Zhou and J. Xu, *J. Hazard. Mater.*, **310**, 235 (2016).
51. S. Álvarez-Torrellas, A. Rodríguez, G. Ovejero and J. García, *Chem. Eng. J.*, **283**, 936 (2016).
52. S. V. Manjunath, R. S. Baghel and M. Kumar, *Chem. Eng. J.*, **381**, 122713 (2020).
53. F. Cao, C. Lian, J. Yu, H. Yang and S. Lin, *Bioresour. Technol.*, **276**, 211 (2019).
54. T. Ai, X. Jiang and Q. Liu, *Open Chem.*, **16**, 842 (2018).